

See discussions, stats, and author profiles for this publication at: <https://www.researchgate.net/publication/263989817>

# Three-Dimensional Porous Spinel Ferrite as an Adsorbent for Pb(II) Removal from Aqueous Solutions

ARTICLE *in* INDUSTRIAL & ENGINEERING CHEMISTRY RESEARCH · NOVEMBER 2013

Impact Factor: 2.59 · DOI: 10.1021/ie303359e

---

CITATIONS

15

---

READS

54

## 2 AUTHORS, INCLUDING:



Seung-Mok Lee

Catholic Kwandong University

125 PUBLICATIONS 1,478 CITATIONS

SEE PROFILE

# Three-Dimensional Porous Spinel Ferrite as an Adsorbent for Pb(II) Removal from Aqueous Solutions

D. Harikishore Kumar Reddy and Seung-Mok Lee\*

Department of Environmental Engineering, Kwandong University, 522 Naegok-dong, Gangneung-si, Gangwon-do 210-701, Republic of Korea

## Supporting Information

**ABSTRACT:** Application of porous magnetic materials for detoxification of pollutants from aqueous solutions has attracted great attention in recent years because of their ease of separation and enhanced efficiency. In this light, a three-dimensional (3D) porous  $\text{NiFe}_2\text{O}_4$  adsorbent (PNA) having significant magnetic properties was synthesized and employed in detoxification of Pb(II) contaminated aqueous solution. The PNA was obtained by a sol–gel process using chitosan as precursor and was fully characterized by using FTIR, XRD, SEM, and EDAX analytical techniques. The surface morphology obtained from the SEM images of the PNA clearly exhibited the three-dimensional porous structure; pores were well interconnected. The kinetic mechanism was best described by pseudo-second-order and double-exponential models. The equilibrium state sorption data was best fitted to the Langmuir and Sips isotherm models. The studies clearly demonstrated that the PNA could be an efficient material for treatment of Pb(II) contaminated wastewaters.

## INTRODUCTION

Water pollution is one of the major environmental threats observed around the globe, consequent upon rapid industrialization and urbanization. The ever-increasing contamination of water bodies with a variety of organic, inorganic, and biological pollutants is one of the key environmental problems. However, among all of these pollutants, heavy metals are notorious water pollutants with high toxicity and reported carcinogenicity.<sup>1,2</sup> Lead is one of the heavy metals of particular concern in the aqueous environment, and its toxicity with its persistency has attracted extensive attention.<sup>3,4</sup> Sources of Pb(II), its effects on the environment and human health, and also permissible limits for Pb(II) by various international and national regulatory bodies are well articulated elsewhere in several reviews.<sup>5–7</sup> Therefore, lead removal from aqueous solutions to protect biodiversity, hydrosphere ecosystems, and human beings is of utmost importance. Conventional technologies reported for the removal of Pb(II) from water environment include chemical precipitation, membrane separation, ion exchange, biological removal, etc.<sup>8</sup> However, rapid, efficient, and economical removal of toxic Pb(II) from the aquatic environment was an important technological challenge. Adsorption is one of the most effective processes of advanced wastewater treatment technologies due to its ease of operation and the availability of a wide range of adsorbents (activated carbons, biomaterials, nanomaterials, industrial byproducts, clays, etc.) assessed previously in the removal of Pb(II) from aqueous solutions.<sup>9–12</sup>

However, some difficulties were encountered in separation and regeneration of used adsorbent for subsequent application. Therefore, the design and exploration of novel adsorbents is a continuous effort for many researchers. In recent years significant effort was devoted to the development of novel magnetic adsorbent materials for effective, efficient, and economical removal of Pb(II).

Magnetic materials were the most attractive class of materials for removal of toxic contaminants due to quick and effective magnetic separation from treated water.<sup>13</sup> Magnetic properties of adsorbent materials are useful for overcoming some of the issues present with filtration, centrifugation, or gravitational separation, and for saving energy.<sup>14–16</sup> Magnetic adsorbents with porous structures possessed significantly high specific surface areas, effectively facilitated mass transfer, and substantially lowered the diffusion resistance. Due to their large surface areas and good adsorption capacities, inorganic porous materials were widely used as adsorbents.<sup>17</sup> Among these materials spinel ferrites were known with unique advantages of magnetic and stable chemical properties. So far, there have been several reports about the applications of spinel ferrites and their composites as adsorbents or catalysts in water treatment.<sup>18–21</sup> Spinel ferrites are represented by the general formula  $\text{MFe}_2\text{O}_4$ , where M is a metal or a group of metallic elements with two different valences.<sup>22</sup> In particular, the  $\text{MFe}_2\text{O}_4$  ( $\text{M} = \text{Mn, Fe, Co, Ni}$ ) ferrites with spinel structure exhibit interesting magnetic, magnetoresistive, and magneto-optical properties that were potentially useful for a broad range of applications. Among spinel ferrites, nickel ferrite ( $\text{NiFe}_2\text{O}_4$ ) was known as a soft magnetic material and was the most important spinel ferrite.  $\text{NiFe}_2\text{O}_4$  with ferromagnetic character was originated from the magnetic moment of antiparallel spins between  $\text{Fe}^{3+}$  ions at tetrahedral sites and  $\text{Ni}^{2+}$  ions at octahedral sites.<sup>23</sup> However, metal ferrites confined with porous structure were an especially interesting class of materials. This structure was combined with key advantages as magnetic ferrite possessed unique magnetic response while

**Received:** December 6, 2012

**Revised:** June 20, 2013

**Accepted:** October 18, 2013

**Published:** October 18, 2013



porous matrixes exhibited highly developed internal specific surface areas, good chemical stability, and high adsorption capacity.<sup>24–26</sup> Furthermore, porous materials with connected pores having irregular and wide pore size distribution, perhaps, provided effective sites for the adsorption process and were likely to be good candidates as adsorbents.<sup>27</sup>

However, to prepare a porous spinel ferrite requires a template material as precursor. Searching for a simple and reliable precursor for the preparation of porous spinel ferrite, chitosan would be an available ligand and template to synthesize porous material. Chitosan could be used as a template to form porous oxides, because the chitosan macromolecule was featured with homogenously well-dispersed and naturally spaced amino groups (~5.8 mmol), providing active surface functional groups to coordinate with metallic species.<sup>28,29</sup> Chitosan (obtained from chitin) next to cellulose is the second most abundant organic resource, imparted rather less expensively.<sup>30</sup> For instance, Kadib et al.<sup>31,32</sup> prepared porous metal oxide microsphere using chitosan as precursor.

The present contribution reports the synthesis of porous material containing spinel nickel ferrite through a sol–gel method and calcination using chitosan as precursor. This method has the advantages of simple preparation, cost effectiveness, and a gentle chemical route resulting in fine porous magnetic material. The objective was to reveal the effectiveness of porous NiFe<sub>2</sub>O<sub>4</sub> adsorbent (PNA) for the removal of Pb(II) from aqueous solution and to study the influence of various parameters on the adsorption process.

## EXPERIMENTAL SECTION

**Materials.** All reagents used in the present investigation were of analytical or equivalent grade and were used without further purification. Chitosan (low molecular weight) was obtained from Aldrich (CAS Registry No. 9012-76-4). Deionized double distilled water was used throughout the experimental studies. The distilled and degassed water was stored in a polyethylene airtight bottle to minimize the mixing of carbon dioxide from atmosphere. Pb(NO<sub>3</sub>)<sub>2</sub> was used for the preparation of 1000 mg/L stock solution.

**Preparation of PNA.** Three-dimensional (3D) porous adsorbent was synthesized by a sol–gel method as reported earlier.<sup>33</sup> In the first step chitosan sol–gel solution (2 wt %) was prepared by dissolving chitosan in 2% (v/v) acetic acid solution and stirring for 2 h. Then, 5.9346 g of Ni(NO<sub>3</sub>)<sub>2</sub>·6H<sub>2</sub>O and 16.4060 g of Fe(NO<sub>3</sub>)<sub>3</sub>·9H<sub>2</sub>O were mixed with 5 mL of water and added slowly into chitosan solution with vigorous stirring. The metal solution occupied the voids of chitosan gel template. The solution was concentrated by heating to 80 °C; the active organic groups of chitosan could react with metal ions (Ni<sup>2+</sup> and Fe<sup>3+</sup>) to form complex precursors. The assembly of Ni<sup>2+</sup>Fe<sup>3+</sup>/chitosan was calcined in a muffle furnace at 400 °C for 5 h, and the organic part was removed. The obtained product was quenched using ice and water to form the 3D porous spinel ferrite. The as-prepared material was washed several times with water, and the final product obtained was denoted as PNA.

**Equipment.** X-ray diffraction (XRD) measurements were carried out using a Rigaku D/MAX 2500 diffractometer equipped with a copper anode (Cu K $\alpha$  = 1.5406 Å) over a scanning interval (2 $\theta$ ) from 20 to 70°. The infrared spectrum of the samples was obtained by using a Fourier transform infrared spectrometer (FT/IR-300E, Jasco, Japan). The sample was prepared as a KBr pellet by investigating the peaks within the

range 4000–400 cm<sup>-1</sup>. The morphology of the solid was observed by scanning electron micrographs obtained by using a Mini-SEM (Mini-SEM, SNE-1500M, Korea). Further, the elemental composition was obtained by using SU-70, Hitachi, Japan.

**Batch Adsorption Assay.** Experimental solutions for the equilibrium tests were prepared from the 1000 mg/L stock solution to the desired concentrations through successive dilutions. To determine the effect pH on adsorption, the experiments were carried out in the initial pH range from 2 to 8 at 298 K with an adsorbent dose of 100 mg and 25 mg L<sup>-1</sup> initial metal ion concentration. The adsorption kinetic studies were obtained using three different metal concentrations (10, 20, and 40 mg/L) from the time intervals 0 to 150 min at 298 K by using the optimum pH 5 and an adsorbent dose of 25 mg. The effect of the initial metal ion concentration (10–600 mg/L) on the removal of Pb(II) was studied from 298 to 308 K. The sample solutions were stirred on a thermostatic mechanical shaker operating at constant speed. After adsorption, the samples were treated with a magnet to separate the PNA adsorbent from the solution and the equilibrium concentration of each solution was analyzed for residual metal concentration using an atomic absorption spectrophotometer. The amount of metal ion retained in the solid phase (adsorbent) was calculated as the difference between the initial concentration of metal solution and the equilibrium concentration of metal ions which was represented in the following equation:

$$q_e = \frac{V(C_0 - C_e)}{m} \quad (1)$$

**Potentiometric Titrations.** Potentiometric titrations were performed in order to determine deprotonation constants and absolute concentrations of specific functional groups present on the sorbent surface. The data may enable the deduction of the pH<sub>PZC</sub> (point of zero charge) of the solid employed. Titrations were performed in a nitrogen atmosphere with 100 mM NaNO<sub>3</sub> electrolyte at room temperature. A quantity of 0.5 g of PNA was suspended in 100 mL of aqueous solution having the known ionic strength 100 mM NaNO<sub>3</sub>, separately in two different beakers. The solutions were titrated separately with 100 mM NaOH or 100 mM HCl. The suspension pH was recorded after each addition of titrant using a digital pH meter, employed prior to its calibration with standard buffers.

**Nonlinear Regression Analysis.** Estimation of the best fit of the kinetic and equilibrium model to the experimental kinetic and equilibrium data is necessary. The typical assessment of the quality models fit to the experimental data is based on the magnitude of the correlation coefficient for the regression. Nonlinear regression analysis was performed in order to determine the model which best fit the experimental results using Origin 8.0 software. The correlation coefficient ( $R^2$ ) and the chi-square value ( $\chi^2$ ) were used to evaluate the “goodness of fit” of curves to the experimental data. The value  $R^2$  represents the percentage of variability in the dependent variable that has been explained by the regression line and may vary from 0 to 1. On the other hand,  $\chi^2$  is basically the sum of the squares of the difference between the experimental data and data obtained from the models, with each square difference divided by the corresponding data obtained by calculation from the models. If the values calculated from the model are similar to the experimental data,  $\chi^2$  should be a small number and vice versa. This can be represented mathematically as

$$\chi^2 = \frac{(\text{experimental value} - \text{model value})^2}{\text{model value}} \quad (2)$$

## RESULTS AND DISCUSSION

**Characterization of the PNA.** *XRD Analysis.* The phase composition of synthesized PNA was investigated by X-ray diffraction analysis and is presented in Figure 1. As can be seen

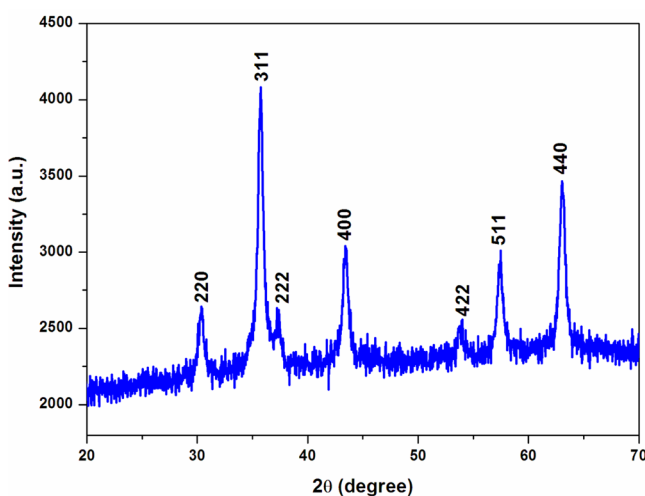


Figure 1. XRD spectrum of PNA.

from the XRD pattern, high intensity and sharp, well-defined peaks indicated the high purity and the high crystalline nature of spinel  $\text{NiFe}_2\text{O}_4$ . No impurity phase was observed in this pattern. The diffraction peaks observed at  $2\theta = 30.42, 35.81, 37.41, 43.46, 54.03, 57.55$ , and  $63.08^\circ$  indicated the planes of (220), (311), (222), (400), (422), (511), and (440), respectively. By referring to the XRD patterns of the standard data (JCPDS 10-0325), all the detected peaks of PNA were indexed with  $\text{NiFe}_2\text{O}_4$  with an inverse spinel structure. The diffraction patterns provide clear evidence of the formation of the pure inverse spinel structure of nickel ferrite.

**FTIR Analysis.** The formation of the porous spinel  $\text{NiFe}_2\text{O}_4$  structure was further supported by comparing the Fourier transform infrared (FTIR) spectra of chitosan (CH) and PNA (Figure 2). The FTIR spectrum of CH possessed major characteristic absorption bands at  $3469\text{ cm}^{-1}$  ( $\text{O}-\text{H}$  and  $\text{N}-\text{H}$  stretching),  $1590$  and  $1654\text{ cm}^{-1}$  ( $\text{N}-\text{H}$  bending vibrations of the secondary amide), and  $1379\text{ cm}^{-1}$  ( $\text{C}-\text{O}$  stretching of amide group). However, a significant difference in the spectral bands was observed after the formation of PNA from chitosan. The strong absorption peaks in the spectral data of PNA at  $3399$  and  $1628\text{ cm}^{-1}$  were assigned to the stretching and bending vibrations of surface hydroxyl groups ( $\text{OH}$ ). The band at  $\sim 590\text{ cm}^{-1}$  corresponds to intrinsic stretching vibrations of the metal at the tetrahedral site ( $\text{Fe}-\text{O}$ , typical of spinel ferrite).<sup>34</sup> Overall, the FTIR spectrum provided supportive evidence for the formation of  $\text{NiFe}_2\text{O}_4$  adsorbent.

**Morphology, Pore Structure, and Elemental Composition.** The morphology of the PNA was investigated by scanning electron microscopy (SEM). Figure 3 provides a comparison of chitosan (CH) and PNA morphology, and it is clearly observed that a marked difference between the surface morphology of chitosan flakes and that of PNA occurred. PNA exhibited 3D porous structure contained highly porous scaffolds with

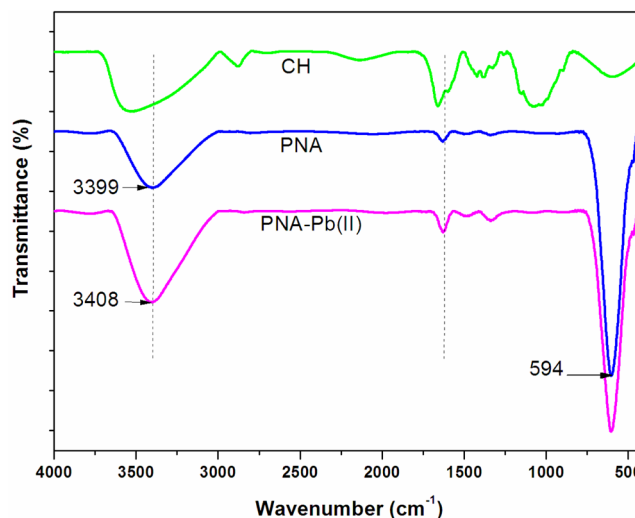
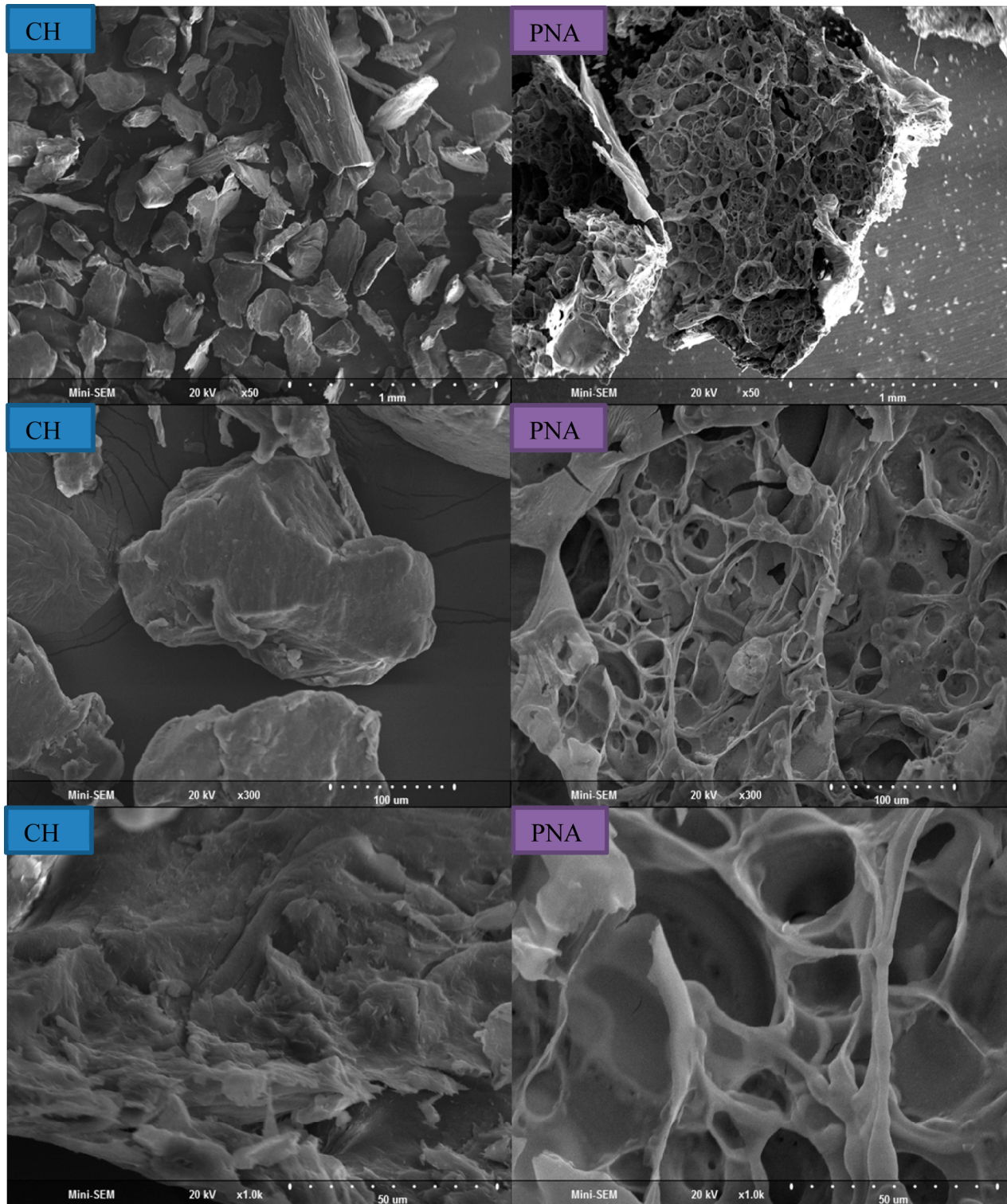


Figure 2. FTIR spectra of chitosan, PNA, and  $\text{Pb}(\text{II})$  loaded PNA.

interconnected porosity. The samples synthesized at  $400\text{ }^\circ\text{C}$  were pure phase of  $\text{NiFe}_2\text{O}_4$  with porous structures, and the average pore size was estimated to be about  $5.0\text{ }\mu\text{m}$ . Further, energy dispersive X-ray analysis (EDAX) was also used to determine the chemical composition of the as-prepared PNA product. The EDAX spectra of the representative samples obtained at an applied potential of  $13\text{ kV}$  and the composition of the elements present in the samples are given in Figure S1 in the Supporting Information. The EDAX results of the as-prepared product PNA showed the existence of Ni, Fe, and O elements with the absence of any impurities. The analysis revealed that Fe and Ni were evenly distributed within the pores and surface of the solid. On the basis of the SEM observations, it was confirmed that the interconnected character of the porosity and the pore size of the scaffolds is suitable for metal ion adsorption.

**Surface characteristics from Potentiometric Titration.** Surface charge characteristics impact the adsorption capacities and adsorption mechanism. Potentiometric titrations were conducted in order to characterize the surface characteristics of PNA adsorbent. Moreover, the potentiometric titration provides the important characteristics of the surface charge properties, i.e., the point of zero charge (PZC) along with the deprotonation constants of the solids (see eqs 3 and 4). The  $\text{pH}_{\text{PZC}}$  was determined and found to be  $7.21$  for PNA. Similarly, the deprotonation constants  $\text{pK}_{\text{a1}}$  and  $\text{pK}_{\text{a2}}$  were found to be  $3.73$  and  $10.69$ , respectively. Further, the total concentration of adsorption sites available on the PNA surface was estimated and was found to be  $2.93 \times 10^{-4}\text{ mol/g}$ , giving the theoretical maximum sorption capacity of  $\text{Pb}(\text{II})$  of  $60.70\text{ mg g}^{-1}$ .

**Effect of pH and Lead Speciation.** The pH values of an aqueous solution play a critical role in the adsorption of metal ions onto an adsorbent. To optimize the pH for maximum removal efficiency, the sorption experiments were conducted in the initial pH range from  $2$  to  $8$  in batch adsorption studies containing  $25\text{ mL}$  of solution with a concentration of  $25\text{ mg L}^{-1}$  metal solution and  $100\text{ mg}$  of PNA (Figure 4a). It was observed that the adsorption of  $\text{Pb}(\text{II})$  onto PNA was strongly pH dependent. The removal efficiency was increased sharply as the pH was increased from  $2.0$  to  $5.0$  and remained nearly  $>90\%$  during the pH region  $5.0$ – $8.0$ . In order to describe the binding of  $\text{Pb}(\text{II})$  onto the functional groups present on the



**Figure 3.** SEM images of chitosan and PNA at different magnifications.

surface of the adsorbent, speciation of Pb(II) was also studied. It was a known fact that the pH influenced the ionization and speciation of metals in aqueous solution. The lead speciation diagram (Figure 4b,c) showed the concentration of dissolved species and the pH at which hydrolysis could occur. The mole fractions were calculated using the Visual MEDUSA speciation program. It was observed that lead predominantly exists as  $\text{Pb}^{2+}$  and  $\text{PbOH}^+$  cations within the pH range from 2.0 to 6.0. The concentration of cationic species, i.e.,  $\text{Pb}^{2+}$ , started to decrease

at pH >6.0 due to its precipitation. A number of other lead species such as  $\text{Pb}_2\text{OH}^{3+}$ ,  $\text{Pb}(\text{OH})_2$ ,  $\text{Pb}(\text{OH})_4^{2-}$ , and  $\text{Pb}(\text{OH})_3^-$  were present in solution between pH 5.0 and 12.0. However, the dominant species were only  $\text{Pb}(\text{OH})_2$  and  $\text{Pb}(\text{OH})_4^{2-}$ .

The surfaces of metal oxides in aqueous medium could acquire a charge by protonation or deprotonation of the neutral sites ( $-\text{OH}$  groups) in accordance with the following reactions

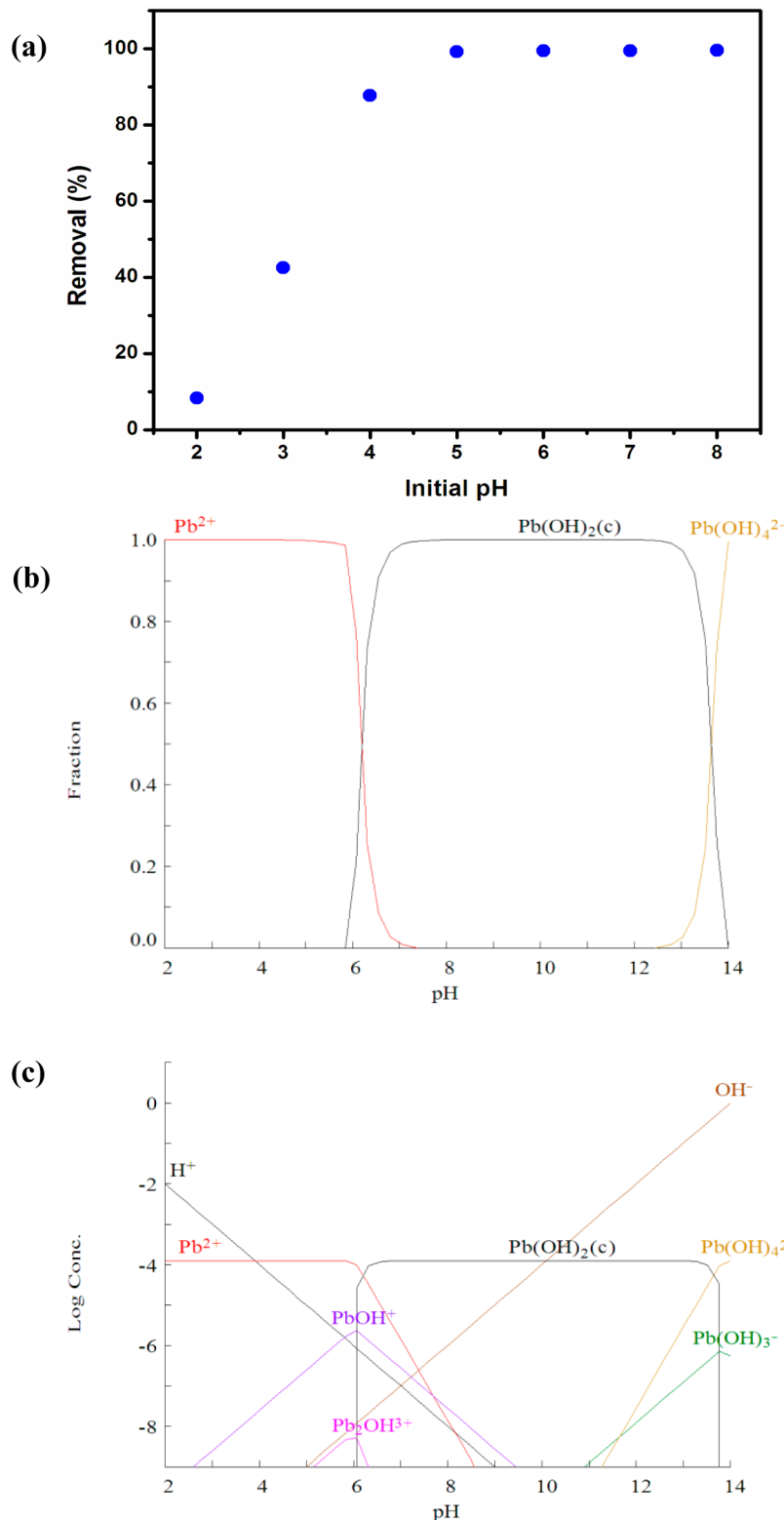
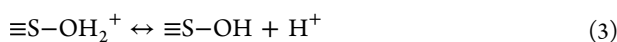


**Figure 4.** (a) Effect of pH on removal of Pb(II) using PNA. Conditions: adsorbent dose, 100 mg; initial concentration, 25 mg L<sup>-1</sup>; temperature, 298 K. (b and c) Speciation of Pb(II).

referring to the two different proton dissociation constants, viz.,  $K_{a1}$  and  $K_{a2}$ :<sup>35</sup>



At lower pH values due to the protonation reaction 3, the concentration of protonated sites are present in higher amount ( $\equiv \text{SOH}_2^+$ ). Otherwise, there would be a competition between protons and metal ions toward the surface hydroxyl groups. Therefore, the adsorption of  $\text{Pb}^{2+}$  and  $\text{PbOH}^+$  was suppressed and hence less uptake of Pb(II) occurred at very low pH values,

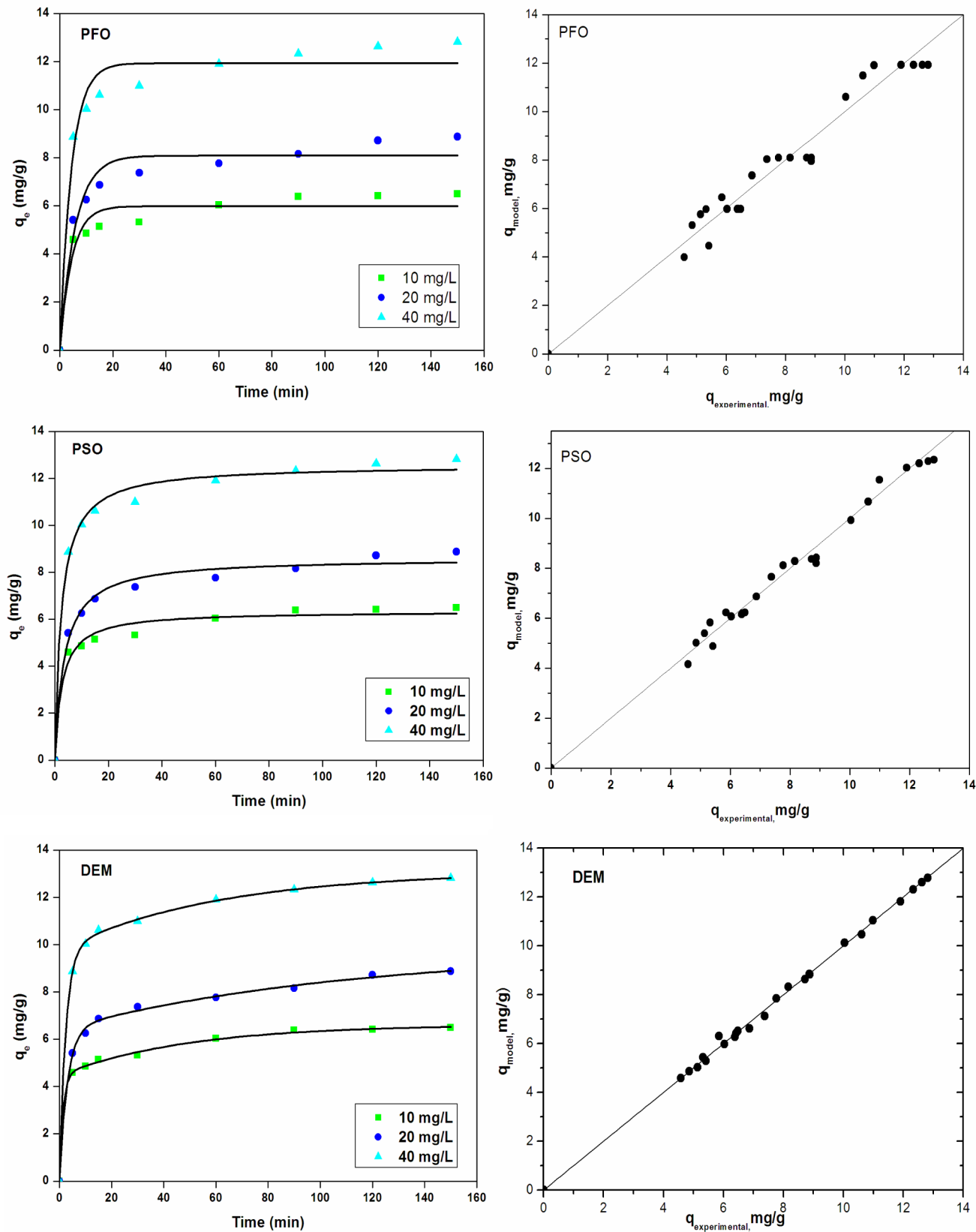


**Figure 5.** Pseudo-first-order, pseudo-second-order, and double-exponential nonlinear kinetic models and comparison of experimental and model adsorption capacities. Conditions: pH, 5.0; adsorbent dose, 25 mg; temperature, 298 K.

i.e.,  $\sim 2.0$ . Lead removal was increased with gradually increasing pH until  $\sim 5.0$ ; such an increase in adsorption was due to the gradual dissociation of surface functional groups since the  $pK_{a1}$

was found to be 3.74. Hence, there was a gradual increase in neutral ( $\equiv \text{SO}$ ) species followed by completely deprotonated sites ( $\equiv \text{SO}^-$ ) species (reaction 4) since the  $pK_{a2}$  obtained was

10.70. This resulted in the surface complexation between  $\text{Pb}^{2+}$  and  $\text{PbOH}^+$ , the surface functional group available on the PNA surface. This, perhaps, facilitated a sharp increase of  $\text{Pb}(\text{II})$  adsorption. At very higher pH values, i.e., beyond  $\text{pH} \sim 6.0$ , the precipitation of  $\text{Pb}(\text{II})$  may contribute to the high uptake of  $\text{Pb}(\text{II})$ . In order to visualize the surface sorption process of  $\text{Pb}(\text{II})$ , the entire adsorption experiments were conducted at  $\text{pH } 5$ .

**Time Profile of Metal Adsorption.** The contact time required for the system to reach equilibrium is an important parameter for designing an adsorption process.<sup>36,37</sup> Experiments were performed at three different initial sorptive concentrations, and data was collected within the time period 0–150 min. Results obtained are depicted in Figure 5, where the solid dots show experimental  $q_t$  values. The maximum adsorption capacity of  $\text{Pb}(\text{II})$  was increased with increasing initial concentration as shown in the Supporting Information (Table S1). It was noted that the fast adsorption process of  $\text{Pb}(\text{II})$  occurred during the first few minutes and an apparent equilibrium was reached within 60 min. The fast adsorption could be ascribed to the 3D pore structure exhibiting more advantages in mass diffusion and transportation.<sup>33</sup> This phenomenon could be explained as follows: the adsorption kinetics is initially fast because the adsorption process takes place predominantly on the outer surface, followed by a slow adsorption step on the inner surface or even the diffusion within the pores of the adsorbent.<sup>38</sup> For the purpose of researching the kinetic mechanism of the adsorption process, a pseudo-first-order (PFO) model,<sup>39</sup> a pseudo-second-order (PSO) model,<sup>40</sup> a double-exponential model (DEM),<sup>41</sup> and an intraparticle diffusion<sup>42</sup> model were applied and the results were compared in specific terms.

**Modeling of the Kinetic Data (PFO, PSO, and DEM).** The kinetics of the adsorption describing the adsorbate uptake rate is one of the important characteristics which control the residence time of adsorbate uptake at the solid–liquid interface.<sup>43</sup> In general, three mechanisms were possible during the adsorption process by porous-adsorbent particles: (i) external mass transfer, (ii) intraparticle transport, and (iii) chemisorption.<sup>44</sup> A pseudo-first-order (PFO) model, a pseudo-second-order (PSO) model, and a double-exponential model (DEM) were used to identify the kinetic behaviors of the adsorption process and the prevailing mechanisms. The applicability of a model was checked by constructing nonlinear plots of  $t$  vs  $q_b$ , and these plots are shown in Figure 5. In Figure 5, the experimental points are shown together with the modeled curves from PFO, PSO, and DEM equations. Whatever the kinetic equation used (Supporting Information, Table S1), the description of the adsorption kinetics was satisfactory. The calculated constants of the three kinetic equations along with  $R^2$  values at different initial  $\text{Pb}(\text{II})$  concentrations are presented in the Supporting Information (Table S1).

Based on the kinetic data (Supporting Information, Table S1) obtained, it was seen that for all the studied concentrations the correlation coefficients for the pseudo-first-order kinetic model were low, which revealed that PFO equation underestimates the  $\text{Pb}(\text{II})$  uptake. Contrary to the PFO equation, the fitting of the kinetic data in the PSO equation showed the best fit with a high correlation coefficient ( $R^2 > 0.97$ ) over the concentration range of 10–40 mg/L. This suggested that the adsorption of  $\text{Pb}(\text{II})$  was not a simple first-order reaction but was a pseudo-second-order reaction. Results were showed that

the data could be described by two-step models as the pseudo-first-order model had correlation coefficients that were not as good as those of the other two models. From the results obtained, it was also observed that the best fits to the experimental data were obtained with the double-exponential and pseudo-second-order models. However, the adsorption of  $\text{Pb}(\text{II})$  seemed to be better described by the double-exponential model.

Adsorbents with a porous structure normally possessed two separate adsorption sites: one at the outer surface which was easily accessible and another inside the pores. The rate of adsorption on the outer surface was more rapid, and that on the inner surface was relatively slower. A double-exponential model equation was applied, and the parameters for the slow and rapid steps and model parameters obtained from experimental data are given in the Supporting Information (Table S1). The model fit very well for all three concentrations ( $R^2 > 0.99$ ), and data shown in Figure 5 confirmed that all of the experimental points coincide with the curve developed by the model. Thus uptake of  $\text{Pb}(\text{II})$  onto PNA material followed the DEM model; according to this model, during the first step, rapid metal uptake took place involving external and internal diffusion. Subsequently, a slow step prevailed; the intraparticle diffusion controlled the adsorption rate and finally the metal uptake reached its equilibrium value. Thus  $K_{D_1}$  and  $K_{D_2}$  were diffusion parameters controlling the overall kinetics. Since there were equal numbers of pore cavities and windows in these materials as shown from SEM studies, diffusion through both structural features supposed to contribute equally. The kinetics was described by two processes with single relaxation times: (a) slow diffusion through windows with high activation energy and (b) fast diffusion along pore cavities with low activation energy.

In fact, to say a kinetic model is effectively fitted to the experimental kinetic data, it is required that the calculated equilibrium adsorption capacity values,  $q_e$  theoretical, should be in accordance with the experimental  $q_e$  values.<sup>45</sup> The values of  $q_e$  theoretical and  $q_e$  experimental for all the applied kinetic models were plotted and are shown in Figure 5. The values of  $q_e$  experimental differed from those of  $q_e$  theoretical (model) from the PFO model, and the values were perfectly in agreement for DEM. Table S1 in the Supporting Information illustrates the calculated values of the kinetic parameters, the related correlation coefficient ( $R^2$ ), and  $\chi^2$  obtained from the three kinetic models. These results suggested that the adsorption of  $\text{Pb}(\text{II})$  on PNA followed the PSO and DEM models.

**Intraparticle Diffusion Modeling.** Adsorption kinetics are usually controlled by different mechanisms, of which the most limiting ones are the diffusion mechanisms. The evaluation of the diffusion mechanism is not possible from the PFO and PSO models. For a solid–liquid adsorption process, the solute transfer process is usually characterized by either external mass transfer (boundary layer diffusion) or intraparticle diffusion or both. Generally, a sorption process is diffusion controlled if its rate is dependent upon the rate at which adsorbate and adsorbent diffuse toward one another. A number of diffusion models have been applied for the defining kinetics of adsorption.<sup>46</sup> In the present investigation the most widely applied Weber and Morris model was used to predict the intraparticle diffusion based mechanism. The Weber–Morris model assumes the following stages: external mass transfer and

stages of intraparticle diffusion in larger and smaller pores until the saturation of the solid surfaces is attained.<sup>47</sup>

For the plot of  $q_t$  versus  $t^{1/2}$  (Figure S2 in the Supporting Information), the modeling exhibited multilinearity, meaning the existence of several steps in the adsorption process. The multilinear plots were divided into three portions. The first sharper portion corresponds to the instantaneous adsorption stage or external surface adsorption. The second portion is the gradual adsorption stage, where intraparticle diffusion is rate-limiting. The third portion is the final equilibrium stage, where intraparticle diffusion starts to slow down due to the extremely low adsorbate concentrations left in the solution. The linear plots at various concentrations do not pass through the origin, which shows that the intraparticle diffusion was not the only rate-controlling step. Other kinetic models may also control the rate of adsorption with all of them operating simultaneously. This was indicative of some degree of boundary layer control. The values of the intercept  $C$  were used for indirect characterization of the boundary layer thickness, which means that the larger the intercept the greater the boundary layer effect.<sup>48</sup> The boundary layer effect on lead complex sorption was more pronounced at high sorptive concentrations (Supporting Information, Table S2), and it increased with increase in initial concentration. The values of the intercept in the Supporting Information (Table S2) provide information about the thickness of the boundary layer and the resistance to the external mass transfer. The larger the intercept that was obtained showed higher external resistance. On the other hand, by increasing the initial metal ion concentration, the actual amount of metal adsorbed per unit mass of PNA was increased. The higher initial concentration of the PNA provided an important driving force to overcome the mass transfer resistance for Pb(II) transfer between the solution and the surface of the PNA. In the process, the Pb(II) primarily encountered the boundary layer effect and then diffused from the boundary layer film onto the adsorbent surface and finally diffused into the porous structure of the adsorbent, which could take a relatively longer contact time. The  $R^2$  values (Supporting Information, Table S2) for this model were lower compared to those obtained from the PFO, PSO, and DEM models. From these results, it was concluded that intraparticle diffusion was not the dominating mechanism for the adsorption of Pb(II) from aqueous solution by PNA. Although the correlation coefficients were high ( $R^2$  values ranged from 0.8727 to 0.9858), the straight line obtained when fitting the experimental data did not pass through the origin, which also indicated that pore diffusion was not only the controlling step.

**Modeling of Sorption Equilibria.** Analysis of equilibrium sorption data is important for optimizing the design of sorption systems, and the adsorption data is modeled using adsorption-type isotherms.<sup>49</sup> The mathematical description of an isotherm relates the concentration of adsorbate in solution  $C_e$  (mg/L) and its accumulation onto adsorbent  $q_e$  (mg/g) at a specific temperature.<sup>50</sup> The distribution of Pb(II) between a solid sorbent and the solution in equilibrium over a range of concentrations at three different temperatures (298–308 K) was studied. During this study the equilibrium data obtained was fitted using four mathematical expressions (Langmuir (L), Freundlich (F), Redlich–Peterson (R–P), and Sips (S)) and is given in the Supporting Information (Table S3). All isotherms were positive and concave to the concentration axis, and the experimental equilibrium values of the amount of Pb(II) sorbed on the PNA was increased with the increase in Pb(II)

concentration in solution. Isotherm data obtained at 308 K is shown in Figure 6. The detailed isotherm parameters for three

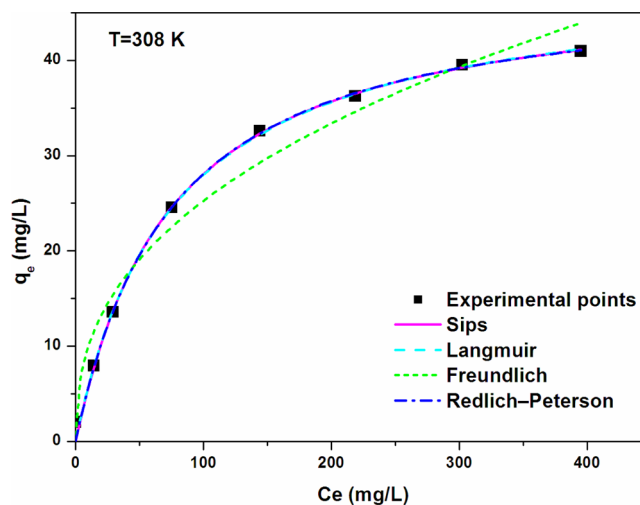


Figure 6. Adsorption isotherms for Pb(II) onto the PNA. Conditions: pH 5.0; adsorbent dose, 100 mg; temperature, 308 K.

different temperatures are compiled in the Supporting Information (Table S3), along with the results of the nonlinear  $\chi^2$  test analysis.

Initially, the two parameter isotherm models Langmuir<sup>51</sup> and Freundlich<sup>52</sup> were applied. Among two-parameter models, high correlation coefficients and low  $\chi^2$  values were observed in the case of the Langmuir model. These results suggest that Pb(II) ions were strongly adsorbed as a monolayer covering the solid adsorbent surface. From the results it was also observed that  $q_m$  parameter from the Langmuir isotherm was increased with increasing temperature. Increasing the temperature is known to increase the rate at which diffusion processes occur. The essential characteristics of the Langmuir isotherm were expressed in terms of a dimensionless separation factor,  $R_L$  ( $R_L = 1/(1 + K_L C_0)$ ), which was then determined at different temperatures over a broad concentration range. The  $R_L$  values were found to vary within a range, 0.925–0.172, 0.909–0.142, and 0.884–0.113 for the temperatures 298, 303, and 308 K, respectively. All the observed  $R_L$  values were found to be between 0 and 1, indicating favorable Pb(II) adsorption onto the PNA. Further, from these results the Freundlich isotherm model was studied, and it indicated that the sorption capacity ( $K_F$ ) was increased with increase in temperature (Supporting Information, Table S3). From the Freundlich model the magnitude of  $1/n$  gives a measure of favorability of adsorption as included in the Supporting Information (Table S3), that the values of  $1/n$  smaller than 1 reflect a favorable adsorption.

Further, the three parameter model Langmuir–Freundlich isotherm, also known as the Sips isotherm,<sup>53</sup> which describes the relationship of the equilibrium concentration of the sorbate between the solid and liquid phases in heterogeneous systems, was employed. At low sorbate concentrations the Sips model effectively reduces the Freundlich isotherm, while at high sorbate concentrations, it predicts a monolayer sorption capacity characteristic of the Langmuir isotherm.<sup>54</sup> This isotherm is capable of modeling both homogeneous and heterogeneous binding surfaces. The value of the exponent  $n_{LF}$  in the Sips equation was  $\approx 1$ , which means that Pb(II) sorption onto the PNA is more of a Langmuir type than of a Freundlich,

since for  $n_{LF} = 1$  the Sips equation reduces to the Langmuir equation in which the variable  $b_{LF}$  corresponds directly to binding affinity ( $K_L$ ). The predicted value of  $q_{\max}$  was lower than the corresponding value ( $q_m$ ) of the Langmuir model (Supporting Information, Table S3). The Redlich–Peterson isotherm<sup>55</sup> also incorporates features of both Langmuir and Freundlich, and the equation was used in further investigation. This model was related with a three-parameter empirical equation and was a hybrid isotherm featuring both Langmuir and Freundlich isotherms.<sup>56</sup> It was used to understand the adsorption mechanism of homogeneous or heterogeneous systems due to its versatility. In this study, the value of the exponent  $b$  was approximately equal to 1, suggesting, like the Sips equation, that the equilibrium data was preferably fitted by the Langmuir model rather the Freundlich. This indicated that the Langmuir condition was the ideal one for the adsorption mechanism.<sup>57</sup> The results of the Redlich–Peterson isotherm also supported the suitability of the Langmuir model.

In order to verify the model for the adsorption system, the data was analyzed using  $\chi^2$  and  $R^2$  analysis. The smaller the error function value and the closer the  $R^2$  value was to unity, the better the curve fitting. The values of errors from the nonlinear method are listed in the Supporting Information (Table S3). The experimental data yielded excellent fitting following the isotherm order Langmuir > Sips > Redlich–Peterson > Freundlich, based on  $R^2$  and  $\chi^2$  values. Among the tested three-parameter equations, the better and perfect representation of the experimental result of the adsorption isotherms was obtained using the Sips model. The maximum adsorption capacities were identical to those obtained using the Langmuir isotherm.

**Effect of Ionic Strength.** Ionic strength is one of the significant parameters that influence the metal ion removal from aqueous solution. Further, it provides significant information about the specific and nonspecific adsorption of metal ions onto the surfaces of solids.<sup>58</sup> In this study, the influence of the ionic strength (sodium nitrate as background electrolyte) on Pb(II) sorption was studied by varying the concentration of sodium nitrate solution from 0.01 to 1.0 mol/L (i.e., 100 times increase). As shown in Figure S3 in the Supporting Information, 100 times increase in ionic strength influenced insignificantly the uptake of Pb(II) by this solid, suggesting that inner sphere complexation reactions account for the adsorption. In the inner sphere surface complexes, the adsorbed molecules or ions and the surface functional groups apparently were sorbed by strong chemical bonds. These results were in accordance with the thermodynamic data showing that an endothermic uptake of Pb(II) by PNA occurred since an increase in temperature favored the uptake of Pb(II), as reported earlier for other divalent metal ions.<sup>59,60</sup>

**Comparison of Adsorption Capacities.** The adsorption capacity is an important factor that determines how much adsorbent is required for quantitative enrichment of the target analyte from a given solution.<sup>61</sup> The maximum adsorption capacity of PNA for the removal of lead was compared with those of other potential adsorbents reported in the literature and was presented in the Supporting Information (Table S4). The maximum adsorption capacity values were based on the Langmuir adsorption capacity.<sup>62–68</sup> The maximum adsorption efficiency of PNA for Pb(II) was found to be 48.98 mg/g; this adsorption capacity was comparable to and moderately higher than that of many other corresponding sorbents reported in the literature. However, higher adsorption capacities of Pb(II) were

reported by some other researchers with different adsorbents. Moreover, the total surface active sites estimated with the help of potentiometric titrations was found to be  $2.93 \times 10^{-4}$  mol/g, and an estimated apparent capacity for Pb(II) was found to be 60.70 mg/g. This value was very comparable to the capacity estimated by this method. Nonetheless, this comparison is not worth emphasizing, since the experimental conditions maintained were different and also combinations of materials employed was different in those studies. Further, the success of any adsorption process in wastewater treatment depends largely on the cost of the adsorbent used. In the present investigation the adsorbent PNA was prepared from the easily available natural biopolymer chitosan in a simple synthetic route. Hence the cost of the adsorbent would likely to be economical when compared with various other adsorbents reported in the literature.

**Adsorption Mechanism.** The two major challenges in the adsorption field were underlined as (i) to prepare the most promising adsorbent from readily available materials and (ii) to identify the sorption mechanism.<sup>68</sup> The present investigation was addressed to fully meet these problems with a wide range of physicochemical parametric studies. The most abundant surface functional group participating in the reactions on PNA surfaces was the hydroxyl group. It was predicted that the surface hydroxyl group (S–OH) were predominantly and preferably involved in surface adsorption of Pb(II) onto the solid surface since the pH<sub>PZC</sub> was found to be 7.22. Further, the involvement of hydroxyl groups was affirmed by the FTIR spectral data (Figure 2). It was found that a peak at  $3399 \text{ cm}^{-1}$  in PNA was observed which corresponds to the hydroxyl groups. However, after adsorption of Pb(II) these groups were shifted to a wavenumber of  $3408 \text{ cm}^{-1}$ ; this confirms the involvement of hydroxyl groups in Pb(II) removal. Along with this from the SEM results it was hypothesized that the presence of pores in the PNA adsorbent further enhances the adsorption of Pb(II).

## CONCLUSIONS

In summary, as-prepared  $\text{NiFe}_2\text{O}_4$  adsorbent with 3D porous structure possesses attractive adsorption properties toward Pb(II) removal from aqueous solutions. The adsorption rate is so fast that it reaches equilibrium in a short time (almost 60 min). This fast adsorption rate comes from the interconnected pore structure of PNA, which is beneficial for the diffusion of metal ions to the adsorption sites on PNA. The adsorption kinetics followed the mechanism of the DEM, evidencing a two-stage adsorption process. From FTIR spectral data it was found that surface hydroxyl groups play a role in the adsorption of lead ions from aqueous solution onto the surface of PNA. Also, the magnetic separation of the PNA from treated Pb(II) solution by a magnet was achieved within 2 min; this is an advantageous property of the as-prepared materials (Figure S4 in the Supporting Information). Moreover, the magnetic adsorbent was easily dispersed in aqueous solution and can be rapidly separated by applying a magnetic field. In conclusion, as-prepared adsorbent PNA showed a promising prospect for treatment of Pb(II) containing wastewater.

## ASSOCIATED CONTENT

### Supporting Information

EDX spectrum of PNA adsorbent, Weber–Morris plots and effect of ionic strength on Pb(II) adsorption, picture showing separation of PNA after adsorption by using a magnet, and

tables representing parameters of kinetics models, isotherm models, and comparison of maximum adsorption capacities of various adsorbents. This material is available free of charge via the Internet at <http://pubs.acs.org>.

## AUTHOR INFORMATION

### Corresponding Author

\*Tel.: +82 33 649 7535. Fax: +82 33 642 7635. E-mail: leesm@kwandong.ac.kr.

### Notes

The authors declare no competing financial interest.

## ACKNOWLEDGMENTS

This work was supported by a National Research Foundation of Korea (NRF) grant funded by the Korean government (MEST) (No. 2012R1A2A4A01001539). This subject is also supported by Korea Ministry of Environment as "Converging technology project".

## NOMENCLATURE

$a_{RP}$  = Redlich-Peterson isotherm constant,  $\text{dm}^3 \text{mg}^{-1}$

$b_{LF}$  = Langmuir-Freundlich isotherm constant,  $\text{dm}^3 \text{mg}^{-1}$

$b_{RP}$  = Redlich-Peterson isotherm exponent

$C$  = intercept from Weber-Morris equation,  $\text{mg g}^{-1}$

$C_0$  = initial concentration of adsorbate in aqueous solution,  $\text{mg/L}$

$C_e$  = concentration of adsorbate in aqueous solution at equilibrium,  $\text{mg/L}$

$D_1$  = sorption constant rate parameter of the rapid step of double-exponential model,  $\text{mmol L}^{-1}$

$D_2$  = sorption constant rate parameter of the slow step of double-exponential model,  $\text{mmol L}^{-1}$

$k_1$  = rate constant of the first-order kinetic model,  $\text{min}^{-1}$

$k_2$  = rate constant of the second-order kinetic model,  $\text{g mg}^{-1} \text{min}^{-1}$

$K_{D_1}$  = parameter of the rapid step of double-exponential model,  $\text{min}^{-1}$

$K_{D_2}$  = parameter of the slow step of double-exponential model,  $\text{min}^{-1}$

$K_F$  = Freundlich isotherm constant,  $(\text{mg g}^{-1})(\text{L mg}^{-1})^{1/n}$

$k_{WM}$  = Weber-Morris kinetic constant,  $\text{mg g}^{-1} \text{min}^{0.5}$

PZC = point of zero charge

$q$  = amount of adsorbate adsorbed,  $\text{mg g}^{-1}$

$q_e$  = mass of adsorbate adsorbed at equilibrium,  $\text{mg/g}$

$q_t$  = amount of sorbate sorbed at time  $t$ ,  $\text{mg g}^{-1}$

$q_{exp}$  = experimental mass of adsorbate adsorbed,  $\text{mg/g}$

$q_{max}$  = maximum biosorption capacity,  $\text{mg g}^{-1}$

$R^2$  = correlation coefficient

$T$  = temperature,  $\text{K}$

$t$  = time,  $\text{min}$

$V$  = volume of the solution,  $\text{Ml}$

$\chi^2$  = chi-square function

## REFERENCES

- Goyer, R. A. *Handbook on Toxicity of Inorganic Compounds*; Marcel Dekker: New York, 1988.
- Reddy, D. H. K.; Seshaiah, K.; Reddy, A. V. R.; Rao, M. M.; Wang, M. C. Biosorption of  $\text{Pb}^{2+}$  from aqueous solutions by *Moringa oleifera* bark: Equilibrium and kinetic studies. *J. Hazard. Mater.* **2010**, *174*, 831–838.
- Meyer, P. A.; Brown, M. J.; Falk, H. Global approach to reducing lead exposure and poisoning. *Mutat. Res.* **2008**, *659*, 166–175.

(4) Reddy, D. H. K.; Harinath, Y.; Seshaiah, K.; Reddy, A. V. R. Biosorption of  $\text{Pb}(\text{II})$  from aqueous solutions using chemically modified *Moringa oleifera* tree leaves. *Chem. Eng. J.* **2010**, *162*, 626–634.

(5) Poręba, R.; Gać, P.; Poręba, M.; Andrzejak, R. Environmental and occupational exposure to lead as a potential risk factor for cardiovascular disease. *Environ. Toxicol. Pharmacol.* **2011**, *31*, 267–277.

(6) Mansouri, M. T.; Cauli, O. Motor alterations induced by chronic lead exposure. *Environ. Toxicol. Pharmacol.* **2009**, *27*, 307–313.

(7) Sud, D.; Mahajan, G.; Kaur, M. P. Agricultural waste material as potential adsorbent for sequestering heavy metal ions from aqueous solutions—A review. *Bioresour. Technol.* **2008**, *99*, 6017–6027.

(8) Fu, F.; Wang, Q. Removal of heavy metal ions from wastewaters: A review. *J. Environ. Manage.* **2011**, *92*, 407–418.

(9) Unuabonah, E. I.; Olu-Owolabi, B. I.; Taubert, A.; Omolehin, E.; Adebawale, K. O. SAPK: A Novel Composite Resin for Water Treatment with very high  $\text{Zn}^{2+}$ ,  $\text{Cd}^{2+}$ , and  $\text{Pb}^{2+}$  Adsorption Capacity. *Ind. Eng. Chem. Res.* **2013**, *52*, 578–585, DOI: 10.1021/ie3024577.

(10) Du, C.; Liu, H.; Xiao, M.; Gao, D.; Huang, D.; Li, Z.; Chen, T.; Mo, J.; Wang, K.; Zhang, C. Adsorption of Iron and Lead Ions from an Aqueous Solution by Plasma-Modified Activated Carbon. *Ind. Eng. Chem. Res.* **2012**, *51*, 15618–15625.

(11) Reddy, D. H. K.; Lee, S.-M.; Seshaiah, K. Biosorption of Toxic Heavy Metal Ions from Water Environment Using Honeycomb Biomass—An Industrial Waste Material. *Water, Air, Soil Pollut.* **2012**, *223*, 5967–5982.

(12) Prasad, M.; Saxena, S.; Amritphale, S. S.; Chandra, N. Kinetics and Isotherms for Aqueous Lead Adsorption by Natural Minerals. *Ind. Eng. Chem. Res.* **2000**, *39*, 3034–3037.

(13) Reddy, D. H. K.; Lee, S.-M. Application of magnetic chitosan composites for the removal of toxic metal and dyes from aqueous solutions. *Adv. Colloid Interface Sci.* **2013**, <http://dx.doi.org/10.1016/j.cis.2013.10.002>.

(14) Yavuz, C. T.; Mayo, J. T.; Yu, W. W.; Prakash, A.; Falkner, J. C.; Yean, S.; Cong, L.; Shipley, H. J.; Kan, A.; Tomson, M.; Natelson, D.; Colvin, V. L. Low-Field Magnetic Separation of Monodisperse  $\text{Fe}_3\text{O}_4$  Nanocrystals. *Science* **2006**, *314*, 964–967.

(15) Polshettiwar, V.; Luque, R.; Fihri, A.; Zhu, H.; Bouhrara, M.; Bassat, J.-M. Magnetically Recoverable Nanocatalysts. *Chem. Rev.* **2011**, *111*, 3036–3075.

(16) Wang, Z.; Liu, X.; Lv, M.; Meng, J. A new kind of mesoporous  $\text{Fe}_7\text{Co}_3/\text{carbon}$  nanocomposite and its application as magnetically separable adsorber. *Mater. Lett.* **2010**, *64*, 1219–1221.

(17) Ji, X.; Liu, Y.; Li, M.; Evans, D. G.; Xu, Q. Synthesis of mesoporous Co-spinel ferrite using a hard template and gaseous diffusion. *Solid State Sci.* **2011**, *13*, 404–408.

(18) Hou, X.; Feng, J.; Ren, Y.; Fan, Z.; Zhang, M. Synthesis and adsorption properties of spongelike porous  $\text{MnFe}_2\text{O}_4$ . *Colloids Surf., A* **2010**, *363*, 1–7.

(19) Ren, Y.; Dong, Q.; Feng, J.; Ma, J.; Wen, Q.; Zhang, M. Magnetic porous ferrospinel  $\text{NiFe}_2\text{O}_4$ : A novel ozonation catalyst with strong catalytic property for degradation of di-n-butyl phthalate and convenient separation from water. *J. Colloid Interface Sci.* **2012**, *382*, 90–96.

(20) Lv, S.; Chen, X.; Ye, Y.; Yin, S.; Cheng, J.; Xia, M. Rice hull/ $\text{MnFe}_2\text{O}_4$  composite: Preparation, characterization and its rapid microwave-assisted COD removal for organic wastewater. *J. Hazard. Mater.* **2009**, *171*, 634–639.

(21) Deraz, N. M.; Alarifi, A.; Shaban, S. A. Removal of sulfur from commercial kerosene using nanocrystalline  $\text{NiFe}_2\text{O}_4$  based sorbents. *J. Saudi Chem. Soc.* **2010**, *14*, 357–362.

(22) Galindo, R.; Mazario, E.; Gutiérrez, S.; Morales, M. P.; Herrasti, P. Electrochemical synthesis of  $\text{NiFe}_2\text{O}_4$  nanoparticles: Characterization and their catalytic applications. *J. Alloys Compd.* **2012**, *S36*, S241–S244.

(23) Kinemuchi, Y.; Ishizaka, K.; Suematsu, H.; Jiang, W.; Yatsui, K. Magnetic properties of nanosize  $\text{NiFe}_2\text{O}_4$  particles synthesized by pulsed wire discharge. *Thin Solid Films* **2002**, *407*, 109–113.

- (24) Li, B.; Cao, H.; Shao, J.; Qu, M.; Warner, J. H. Superparamagnetic  $\text{Fe}_3\text{O}_4$  nanocrystals@graphene composites for energy storage devices. *J. Mater. Chem.* **2011**, *21*, 5069–5075.
- (25) Xu, S.; Zhang, F.; Kang, Q.; Liu, S.; Cai, Q. The effect of magnetic field on the catalytic graphitization of phenolic resin in the presence of Fe–Ni. *Carbon* **2009**, *47*, 3233–3237.
- (26) White, R. J.; Luque, R.; Budarin, V. L.; Clark, J. H.; Macquarrie, D. J. Supported metal nanoparticles on porous materials. Methods and applications. *Chem. Soc. Rev.* **2009**, *38*, 481–494.
- (27) Ren, Y.; Li, N.; Feng, J.; Luan, T.; Wen, Q.; Li, Z.; Zhang, M. Adsorption of Pb(II) and Cu(II) from aqueous solution on magnetic porous ferrospinel  $\text{MnFe}_2\text{O}_4$ . *J. Colloid Interface Sci.* **2012**, *367*, 415–421.
- (28) Guibal, E. Heterogeneous catalysis on chitosan-based materials: a review. *Prog. Polym. Sci.* **2005**, *30*, 71–109.
- (29) Agrawal, P.; Strijkers, G. J.; Nicolay, K. Chitosan-based systems for molecular imaging. *Adv. Drug Delivery Rev.* **2010**, *62*, 42–58.
- (30) Yang, M.; Yang, Y.; Liu, B.; Shen, G.; Yu, R. Amperometric glucose biosensor based on chitosan with improved selectivity and stability. *Sens. Actuators, B* **2004**, *101*, 269–276.
- (31) Kadib, A. E.; Molvinger, K.; Bousmina, M.; Brunel, D. Decoration of chitosan microspheres with inorganic oxide clusters: Rational design of hierarchically porous, stable and cooperative acid–base nanoreactors. *J. Catal.* **2010**, *273*, 147–155.
- (32) Kadib, A. E.; Molvinger, K.; Cacciaguerra, T.; Bousmina, M.; Brunel, D. Chitosan templated synthesis of porous metal oxide microspheres with filamentary nanostructures. *Microporous Mesoporous Mater.* **2011**, *142*, 301–307.
- (33) Hou, X.; Feng, J.; Liu, X.; Ren, Y.; Fan, Z.; Wei, T.; Meng, J.; Zhang, M. Synthesis of 3D porous ferromagnetic  $\text{NiFe}_2\text{O}_4$  and using as novel adsorbent to treat wastewater. *J. Colloid Interface Sci.* **2011**, *362*, 477–485.
- (34) Maensiri, S.; Masingboon, C.; Boonchom, B.; Seraphin, S. A simple route to synthesize nickel ferrite ( $\text{NiFe}_2\text{O}_4$ ) nanoparticles using egg white. *Scr. Mater.* **2007**, *56*, 797–800.
- (35) Musić, S.; Ristic, M. Adsorption of zinc(II) on hydrous iron oxides. *J. Radioanal. Nucl. Chem.* **1992**, *162*, 351–362.
- (36) Reddy, D. H. K.; Ramana, D. K. V.; Seshaiah, K.; Reddy, A. V. R. Biosorption of Ni(II) from aqueous phase by *Moringa oleifera* bark, a low cost biosorbent. *Desalination* **2011**, *268*, 150–157.
- (37) Witek-Krowiak, A.; Reddy, D. H. K. Removal of microelemental Cr(III) and Cu(II) by using soybean meal waste—Unusual isotherms and insights of binding mechanism. *Bioresour. Technol.* **2013**, *127*, 350–357.
- (38) Cooney, D. O. *Adsorption Design for Wastewater Treatment*; CRC Press: Boca Raton, FL, 1999.
- (39) Lagergren, S. About the theory of so-called adsorption of soluble substances. *K. Svens. Vetenskapsakad. Handl.* **1898**, *24*, 1–39.
- (40) Ho, Y. S. Second-order kinetic model for the sorption of cadmium onto tree fern: A comparison of linear and non-linear methods. *Water Res.* **2006**, *40*, 119–125.
- (41) Wilczak, A.; Keinath, T. M. Kinetics of sorption and desorption of copper(II) and lead(II) on activated carbon. *Water Environ. Res.* **1993**, *65*, 238–244.
- (42) Weber, W. J.; Morris, J. C. Kinetics of adsorption on carbon from solution. *J. Sanit. Eng. Div., Am. Soc. Civ. Eng.* **1963**, *89*, 31–59.
- (43) Zhu, J.; Wei, S.; Gu, H.; Rapole, S. B.; Wang, Q.; Luo, Z.; Haldolaarachchige, N.; Young, D. P.; Guo, Z. One-Pot Synthesis of Magnetic Graphene Nanocomposites Decorated with Core@Double-shell Nanoparticles for Fast Chromium Removal. *Environ. Sci. Technol.* **2011**, *46*, 977–985.
- (44) Lv, L.; He, J.; Wei, M.; Evans, D. G.; Duan, X. Uptake of chloride ion from aqueous solution by calcined layered double hydroxides: Equilibrium and kinetic studies. *Water Res.* **2006**, *40*, 735–743.
- (45) Ünlü, N.; Ersoz, M. Adsorption characteristics of heavy metal ions onto a low cost biopolymeric sorbent from aqueous solutions. *J. Hazard. Mater.* **2006**, *136*, 272–280.
- (46) Witek-Krowiak, A. Analysis of temperature-dependent biosorption of  $\text{Cu}^{2+}$  ions on sunflower hulls: Kinetics, equilibrium and mechanism of the process. *Chem. Eng.* **2012**, *192*, 13–20.
- (47) Witek-Krowiak, A. Analysis of influence of process conditions on kinetics of malachite green biosorption onto beech sawdust. *Chem. Eng.* **2011**, *171*, 976–985.
- (48) Özcan, A.; Öncü, E. M.; Özcan, A. S. Adsorption of Acid Blue 193 from aqueous solutions onto DEDMA-sepiolite. *J. Hazard. Mater.* **2006**, *129*, 244–252.
- (49) Khambhaty, Y.; Mody, K.; Basha, S.; Jha, B. Kinetics, equilibrium and thermodynamic studies on biosorption of hexavalent chromium by dead fungal biomass of marine *Aspergillus niger*. *Chem. Eng. J.* **2009**, *145*, 489–495.
- (50) Wang, L.-H.; Lin, C.-I. Equilibrium study on chromium(III) ion removal by adsorption onto rice hull ash. *J. Taiwan Inst. Chem. Eng.* **2009**, *40*, 110–112.
- (51) Langmuir, I. The constitution and fundamental properties of solids and liquids. Part I. Solids. *J. Am. Chem. Soc.* **1916**, *38*, 2221–2295.
- (52) Freundlich, H. Over the adsorption in solution. *Z. Phys. Chem.* **1906**, *57*, 385–470.
- (53) Sips, R. On the structure of a catalyst surface. *J. Chem. Phys.* **1948**, *16*, 490–495.
- (54) Ho, Y. S.; Porter, J. F.; McKay, G. Equilibrium isotherm studies for the sorption of divalent metal ions onto peat: copper, nickel and lead single component systems. *Water, Air, Soil Pollut.* **2002**, *141*, 1–33.
- (55) Redlich, O.; Peterson, D. L. A useful adsorption isotherm. *J. Chem. Phys.* **1959**, *63*, 1024.
- (56) Gimbert, F.; Morin-Crini, N.; Renault, F.; Badot, P.-M.; Crini, G. Adsorption isotherm models for dye removal by cationized starch-based material in a single component system: Error analysis. *J. Hazard. Mater.* **2008**, *157*, 34–46.
- (57) Reddy, D. H. K.; Lee, S.-M. Synthesis and characterization of a chitosan ligand for the removal of copper from aqueous media. *J. Appl. Polym. Sci.* **2013**, *130*, 4542–4550.
- (58) Lee, S.-M.; Laldawngiana, C.; Tiwari, D. Iron oxide nanoparticles-immobilized-sand material in the treatment of Cu(II), Cd(II) and Pb(II) contaminated waste waters. *Chem. Eng. J.* **2012**, *195*–196, 103–111.
- (59) Mishra, S. P.; Tiwari, D.; Dubey, R. S. The uptake behaviour of rice (Jaya) husk in the removal of Zn(II) ions—A radiotracer study. *Appl. Radiat. Isot.* **1997**, *48*, 877–882.
- (60) Mishra, S. P.; Dubey, S. S.; Tiwari, D. Inorganic particulates in removal of heavy metal toxic ions: IX. Rapid and efficient removal of Hg(II) by hydrous manganese and tin oxides. *J. Colloid Interface Sci.* **2004**, *279*, 61–67.
- (61) Wang, L.; Tian, C.; Mu, G.; Sun, L.; Zhang, H.; Fu, H. Magnetic nanoparticles/graphitic carbon nanostructures composites: Excellent magnetic separable adsorbents for precious metals from aqueous solutions. *Mater. Res. Bull.* **2012**, *47*, 646–654.
- (62) Roy, A.; Bhattacharya, J. Removal of Cu(II), Zn(II) and Pb(II) from water using microwave-assisted synthesized maghemite nanotubes. *Chem. Eng. J.* **2012**, *211*–212, 493–500.
- (63) Tan, Y.; Chen, M.; Hao, Y. High efficient removal of Pb(II) by amino-functionalized  $\text{Fe}_3\text{O}_4$  magnetic nano-particles. *Chem. Eng. J.* **2012**, *191*, 104–111.
- (64) Fan, L.; Luo, C.; Sun, M.; Li, X.; Qiu, H. Highly selective adsorption of lead ions by water-dispersible magnetic chitosan/graphene oxide composites. *Colloids Surf., B* **2013**, *103*, 523–529.
- (65) Zhang, Y.; Liu, W.; Zhang, L.; Wang, M.; Zhao, M. Application of bifunctional *Saccharomyces cerevisiae* to remove lead(II) and cadmium(II) in aqueous solution. *Appl. Surf. Sci.* **2011**, *257*, 9809–9816.
- (66) Nassar, N. N. Rapid removal and recovery of Pb(II) from wastewater by magnetic nanoadsorbents. *J. Hazard. Mater.* **2010**, *184*, 538–546.
- (67) Tran, H. V.; Tran, L. D.; Nguyen, T. N. Preparation of chitosan/magnetite composite beads and their application for removal

of Pb(II) and Ni(II) from aqueous solution. *Mater. Sci. Eng., C* **2010**, *30*, 304–310.

(68) Xu, M.; Zhang, Y.; Zhang, Z.; Shen, Y.; Zhao, M.; Pan, G. Study on the adsorption of Ca<sup>2+</sup>, Cd<sup>2+</sup> and Pb<sup>2+</sup> by magnetic Fe<sub>3</sub>O<sub>4</sub> yeast treated with EDTA dianhydride. *Chem. Eng. J.* **2011**, *168*, 737–745.